Interpolation Errors in Wind Fields as a Function of Spatial and Temporal Resolution and Their Impact on Different Types of Kinematic Trajectories

ANDREAS STOHL, GERHARD WOTAWA, PETRA SEIBERT, AND HELGA KROMP-KOLB

Institute of Meteorology and Geophysics, University of Vienna, Vienna, Austria

(Manuscript received 15 December 1994, in final form 6 March 1995)

ABSTRACT

This paper discusses some of the uncertainties that influence kinematic trajectory calculations. The interpolation errors due to different interpolation schemes are examined by degrading high-resolution wind fields from a numerical weather prediction model with respect to space and time. Under typical circumstances, the greatest errors are due to temporal interpolation, followed by horizontal and vertical interpolation. Relative errors in the vertical wind are higher than those in the horizontal wind components. These errors are quite substantial and severely affect the accuracy of trajectories. For instance, a decrease of the temporal resolution from 3 to 6 h leads to average relative interpolation errors of 16% in the horizontal wind components and 40% in the vertical wind component. These errors cause mean transport deviations of 280 km for two-dimensional model-level trajectories and 600 km for three-dimensional trajectories after 96-h travel time. The substantial deviations for three-dimensional trajectories are due to the large interpolation errors of the vertical velocity component. Although the three-dimensional trajectories are more sensitive to interpolation errors, for sufficiently (though not ideally) resolved wind fields they seem to be superior to model-level trajectories. An intercomparison of three-dimensional, model-level, isentropic, and boundary layer trajectories is presented.

1. Introduction

Trajectories computed from meteorological fields are a widely used tool for the description of transport processes in the atmosphere and the understanding of flow structures in moving systems. In the environmental sciences for instance, trajectories are used to examine source–receptor relationships of air pollutants using either statistical methods (e.g., Dorling et al. 1992; Stohl and Kromp-Kolb 1994) or coupled physical–chemical models (e.g., Eliassen and Saltbones 1983; De Leeuw et al. 1990). Therefore, it is of great importance to minimize the errors of calculated trajectories and to know their uncertainties.

Several authors addressed the overall uncertainty of trajectories. One widely used and straightforward method is to compare computed trajectories with trajectories derived from tetroon flights (e.g., Reisinger and Mueller 1983). A major problem of this method is that tetroons follow constant density surfaces while air parcels tend to follow isentropic surfaces. Another drawback is that tetroons are usually tracked only for approximately 100 km and therefore cannot be used to investigate the uncertainty of long-range trajectories. A second frequently used method is the comparison of computed trajectories with trajectories derived from instantaneous tracer releases. Conservative dynamical quantities like potential vorticity (Artz et al. 1985) as well as material tracers like Saharan dust (Martin et al. 1990), smoke from the Kuwaiti oil fires (McQueen and Draxler 1994), and radioactive emissions from Chernobyl (Klug 1992) have been used. Many comparisons have been done with planned releases of tracer gases, because in this case the experimental conditions can be controlled better than when using "tracers of opportunity." Haagenson et al. (1987) concluded that the average root-mean-square (rms) separation between computed and tracer-derived trajectories was approximately 200 km after 24-h travel time. Haagenson et al. (1990) again found a rms separation of somewhat less than 200 km day^{-1}. Draxler (1987) found the fastest growth of trajectory error within the first 24-h travel time, while afterward the growth of the error levels off and is less than 200 km day^{-1}.

A number of independent factors determine the overall accuracy of kinematic trajectories. Probably the most important factor is analysis or forecast errors in the wind field data. The effect of these errors on the accuracy of the trajectories is difficult to assess. Another source of error is the interpolation. Kahl and Samson (1986) used nonoperational high-resolution measurements and several interpolation techniques to quantify errors produced by imprecise interpolation of low-resolution regular observation data. They found errors of about 2–4 m s^{-1} in horizontal wind components and

Corresponding author address: Dr. Andreas Stohl, Institute of Meteorology and Geophysics, Department of Environmental Meteorology, University of Vienna, Hohe Warte 38, A-1190 Wien, Austria. E-mail: ANDREAS@ZAUMSUN1.ZAMG.AC.AT

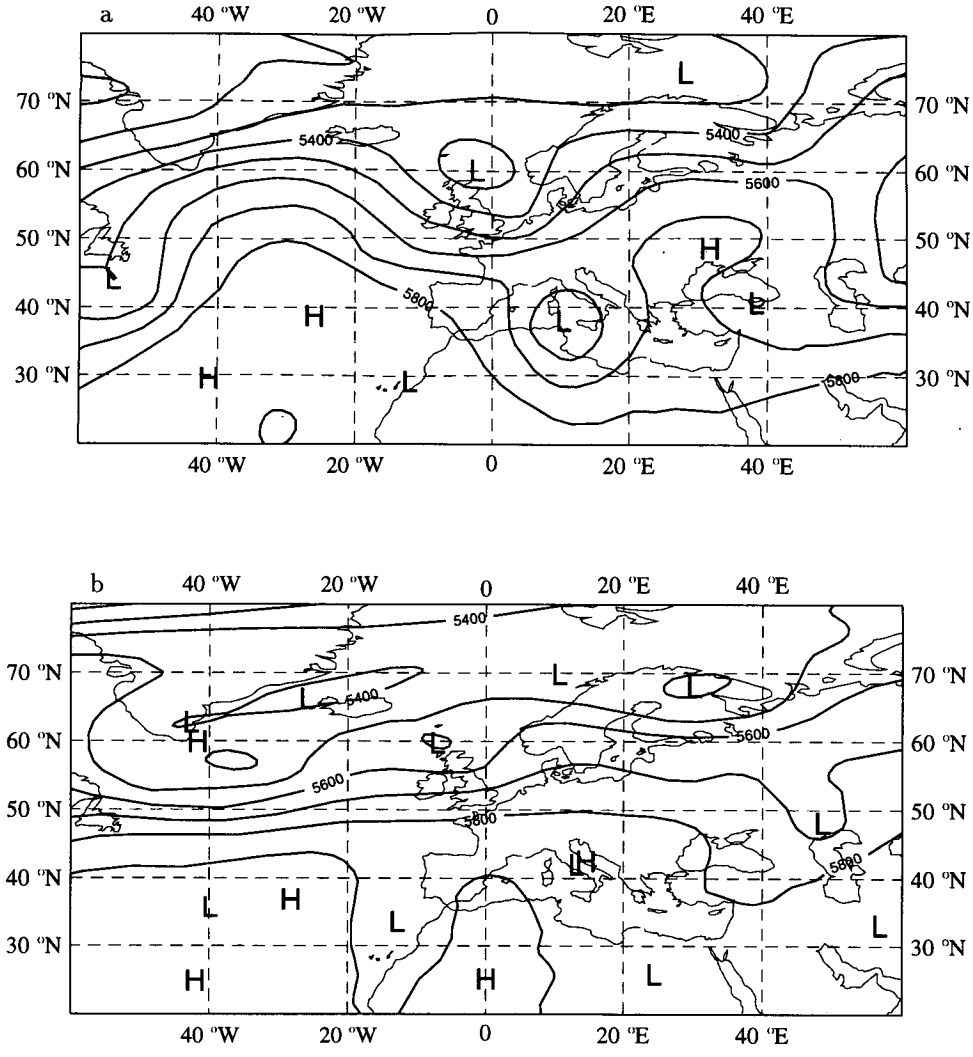

FIG. 1. Isolines of the geopotential on the 500-hPa surface at 1200 UTC for (a) 1 May 1992, (b) 1 August 1992, (c) 1 November 1992, and (d) 1 February 1993.

postulated that this would lead to a 350-km median position error of boundary layer trajectories after 72 h. Kahl et al. (1989) compared trajectories computed from different data sources. After 120-h travel time they found a mean separation of more than 1000 km.

However, even with perfectly analyzed wind fields the computation of trajectories is subject to error sources (Walmsley and Mailhot 1983) such as truncation error of the numerical integration scheme, failure of convergence (Seibert 1993), and interpolation errors. Interpolation from a regular grid to the actual trajectory position is necessary both in space and time. While the truncation error can be kept below any limit by using a sufficiently small time step, interpolation errors pose a major problem. The first part of this work will therefore address the magnitude of these interpolation errors and their effects on trajectory accuracy using analyzed wind fields from a numerical weather prediction model. A similar method was applied by Kuo et al. (1985) and Rolph and Draxler (1990).

Another serious problem is the selection of the most appropriate trajectory type for a given problem. Several types of trajectories have been used, such as isobaric, isentropic, three-dimensional (3D), boundary layer trajectories, etc. (e.g., Danielsen 1961; Martin et al. 1987). They may be constructed either by kinematic or by dynamic methods (Petterssen 1940; Danielsen 1961; Merrill et al. 1986).

The differences between these trajectory types lie in the treatment of vertical velocity. Three different approaches can be found: neglection of vertical motions, selection of a coordinate system in which motions are approximately two-dimensional, and explicit incorporation of the vertical velocity component. Isobaric trajectories belong to the first and obviously crudest approach. Two-dimensional trajectories on terrain-

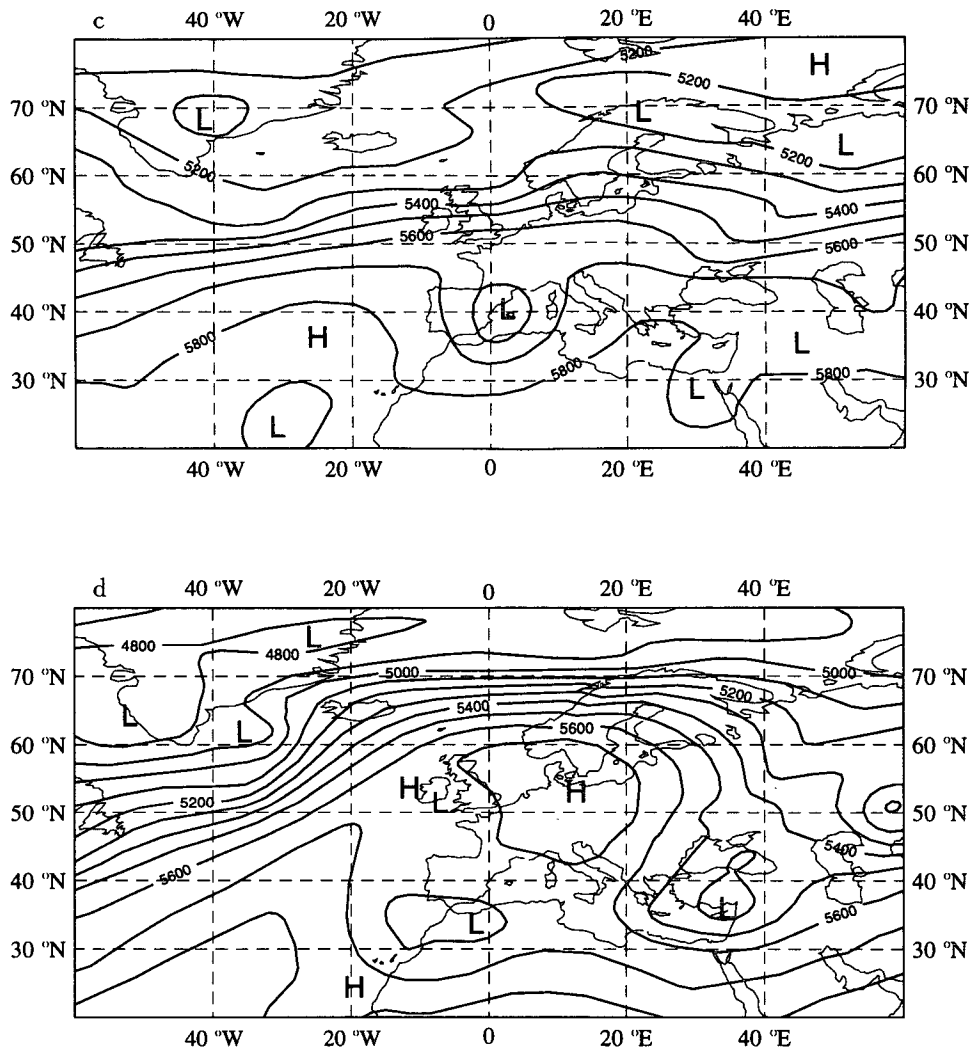

FIG. 1. (*Continued*)

following coordinates obviously are a better approximation in mountainous areas, but they ignore vertical motions of synoptic origin. In isentropic coordinates, trajectories are truly two-dimensional under adiabatic and inviscid conditions. Problems occur near the ground and in saturated moist air. Fully three-dimensional trajectories using dynamically balanced velocities from a numerical model seem to be the best choice.

In a layer with strong mixing, the concept of a trajectory as the path of an air parcel is no more applicable as such a parcel loses its identity due to turbulent mixing. Several authors have approached this problem by calculating trajectories with the wind velocity averaged over the mixed region. In the tracer experiments of Haagenson et al. (1987, 1990), this method yielded the most accurate results in the boundary layer.

Technical constraints may limit the choice of trajectory types for specific applications. Therefore, another aim of this paper is an intercomparison of several types of trajectories.

2. The trajectory model

The trajectory model FLEXTRA was recently developed at the Institute of Meteorology and Geophysics, University of Vienna (requests may be directed to the authors). With slight modifications it can be applied to almost any kind of gridded wind fields. For the integration of the trajectory equation

$$\frac{d\mathbf{X}}{dt} = \mathbf{v}[\mathbf{X}(t)], \tag{1}$$

with t being time, $\mathbf{X}$ the position vector, and $\mathbf{v}$ the wind vector, the iterative scheme after Petterssen (1940) is used:

TABLE 1. Mean absolute (ϵ_a) and relative errors (ϵ_r) of the horizontal interpolation for the wind components u, v, and w. Absolute errors for u and v are given in meters per second and for w in pascals per second. Relative errors are given in percent. The first column is the resolution of the coarse grid in degrees, the first row the interpolation method as described in the text.

		NN		LWD		BI		QU		BC	
		ϵ_a	ϵ_r	ϵ_a	ϵ_r	ϵ_a	ϵ_r	ϵ_a	ϵ_r	ϵ_a	ϵ_r
1.0	u	0.66	19.8	0.32	11.3	0.14	5.6	0.09	3.9	0.06	2.9
	v	0.54	20.8	0.27	12.0	0.12	6.0	0.08	4.3	0.06	3.2
	w	0.049	48.9	0.031	37.3	0.022	27.6	0.020	25.9	0.016	21.8
1.5	u	0.85	25.1	0.57	18.6	0.33	11.9	0.24	9.4	0.21	8.3
	v	0.70	26.3	0.47	19.4	0.28	12.5	0.20	9.9	0.18	8.9
	w	0.061	60.7	0.055	59.4	0.046	50.7	0.044	47.9	0.042	46.4
2.0	u	1.23	33.1	0.83	25.1	0.56	18.1	0.47	15.8	0.42	14.5
	v	1.02	34.6	0.68	25.9	0.46	18.7	0.37	16.2	0.34	15.0
	w	0.084	75.2	0.073	74.3	0.066	67.2	0.067	65.1	0.064	63.9
3.0	u	1.78	43.1	1.36	36.4	1.04	29.3	0.96	27.6	0.90	26.3
	v	1.47	45.0	1.08	37.0	0.84	30.1	0.75	27.8	0.70	26.5
	w	0.111	91.0	0.097	93.2	0.093	88.0	0.099	86.5	0.096	86.0

$$\mathbf{X}_1 = \mathbf{X}_0 + \Delta t \mathbf{v}(\mathbf{X}_0, t),$$

$$\mathbf{X}_n = \mathbf{X}_0 + \frac{\Delta t}{2}[\mathbf{v}(\mathbf{X}_0, t) + \mathbf{v}(\mathbf{X}_{n-1}, t + \Delta t)], \quad (2)$$

where Δt is the integration time step, $\mathbf{X}_0$ is the initial position vector, and $\mathbf{X}_1$ and $\mathbf{X}_n$ are the position vectors at iterations 1 and n, respectively. Another integration scheme described by Pudykiewicz et al. (1985) and investigated by Seibert (1993) is also available within FLEXTRA; it has been found to yield practically the same results with the implemented short time steps but needs slightly more computing time.

The FLEXTRA model uses a flexible integration time step Δt that has to fulfill the Courant–Friedrichs–Lewy criterion $C < 1$ (here $C = 0.2$) with $C = v_i \Delta t / \Delta x_i$, where Δx_i are the grid distances and v_i are the wind components in horizontal and vertical directions, respectively. In addition, the condition $\Delta t = C\Delta T$ was imposed, where ΔT is the temporal resolution of the wind fields. This guarantees that the smallest features resolved by the wind fields are reproduced by the trajectory computation. The short time step resulting from these conditions also ensures that the truncation error remains negligible as compared to the interpolation error.

Within one run of the FLEXTRA model, it is possible to compute several types of trajectories at the same time. The trajectory types being available depend on the meteorological database:

TABLE 2. CPU time requirements on a Sun SPARCstation 10 (relative units) of the five interpolation methods discussed in the text.

Method	NN	LWD	BI	QU	BC
CPU	1	5	3	15	36

- Three-dimensional trajectories are computed using all three wind components.
- By constraining the vertical wind component to equal zero, trajectories on model levels (henceforth called isoeta trajectories) can be constructed. In this case, the air parcels follow the model surfaces. In many weather prediction models the vertical coordinate is chosen such that the lowest model surfaces and thus isoeta trajectories are following the terrain.
- For isentropic trajectories, only the horizontal wind components are used. They are taken from a height that is determined by the condition that the potential temperature remains constant along the trajectory. During unstable conditions, the mean wind of the unstable layer is used for the trajectory calculation.
- For isobaric trajectories, the horizontal wind components were interpolated to the prescribed pressure levels.

TABLE 3. Mean absolute (ϵ_a) and relative errors (ϵ_r) of the vertical interpolation for the wind components u, v, and w. Absolute errors for u and v are given in meters per second and for w in pascals per second. Relative errors are given in percent. The first column gives the number of vertical levels of the coarse grid.

		NN		LI		QU	
		ϵ_a	ϵ_r	ϵ_a	ϵ_r	ϵ_a	ϵ_r
9 levels	u	0.63	15.2	0.19	6.4	0.18	6.1
	v	0.55	17.3	0.19	7.9	0.18	7.5
	w	0.018	36.0	0.006	14.0	0.005	12.8
5 levels	u	1.19	27.7	0.94	22.9	0.65	18.1
	v	1.04	31.1	0.93	27.0	0.65	22.2
	w	0.035	61.5	0.033	42.9	0.021	37.7
3 levels	u	2.57	49.2	2.14	43.0	1.43	34.9
	v	2.04	51.9	1.95	47.8	1.35	40.1
	w	0.072	100.0	0.091	82.2	0.056	73.4

TABLE 4. Same as Table 3 but for the temporal interpolation. The first column gives the temporal resolution.

		NN		LI		QU	
		ϵ_a	ϵ_r	ϵ_a	ϵ_r	ϵ_a	ϵ_r
6 h	u	0.84	19.3	0.52	13.8	0.56	14.6
	v	0.89	24.6	0.54	17.3	0.57	18.0
	w	0.048	46.5	0.038	41.7	0.040	42.2
12 h	u	1.65	35.4	1.30	29.7	1.01	23.4
	v	1.75	44.2	1.36	38.7	1.06	29.6
	w	0.079	72.9	0.069	70.5	0.059	58.0

- So-called boundary layer (BL) trajectories are computed from the vertically averaged horizontal wind within the BL:

$$\bar{v} = \frac{1}{p_h - p_s} \int_{p_s}^{p_h} \mathbf{v}\, dp, \qquad (3)$$

where p_h is the pressure at the top of the BL and p_s is the surface pressure. Boundary layer heights can be either directly computed from model data or set to a climatological mean value.

If a trajectory of any kind reaches the lowest or the uppermost level of the model, it is continued at this level until vertical motion takes it back into the computation grid.

For this investigation, meteorological fields from the global spectral model with 31 vertical levels and 213 resolvable waves of the European Centre for Medium-Range Weather Forecasts (ECMWF) were used (ECMWF 1989). Initialized analyses were available with a temporal resolution of 6 h (0000, 0600, 1200, 1800 UTC) and a horizontal resolution of 0.5°. In addition, 3-h prognostic wind fields from the ECMWF were used for times for which analyzed wind fields were not available (0300, 0900, 1500, 2100 UTC). In the vertical, a hybrid η coordinate system with 31 layers is used. The conversion from η to pressure coordinates is given by $p_k = A_k + B_k p_s$, and the heights of the η surfaces are defined by $\eta_k = A_k/p_0 + B_k$, where η_k is the value of η in the kth level, p_s is the surface pressure, p_0 is a pressure constant (101 325 Pa), and A_k and B_k are coefficients that are chosen in such a way that the levels closest to the ground follow the topography, while the highest levels coincide with pressure surfaces, and levels in between have a gradual transition between these two extremes.

3. Wind field interpolation methods and errors

In this section, errors in the wind fields caused by interpolation in space and time will be examined. The wind fields given on a grid with a resolution of 0.5° and 3 h were used as a reference. This is the highest resolution available from ECMWF. Subsequently, the grid resolution was reduced and the data on the fine grid were reconstructed by interpolation, leading to interpolation errors. An absolute interpolation error ϵ_a was defined by

$$\epsilon_a(x, y, z, t) = |s_r(x, y, z, t) - s_i(x, y, z, t)|, \qquad (4)$$

where s_r is the reference value and s_i is the interpolated value of a quantity s at the same position and time (s can be either the u, v, or w wind component). For the grid points of the fine mesh that coincide with those of the coarse mesh, no interpolation is necessary and thus ϵ_a is zero by definition, while for the rest of the fine mesh grid points interpolation errors occur. A relative interpolation error ϵ_r was defined by

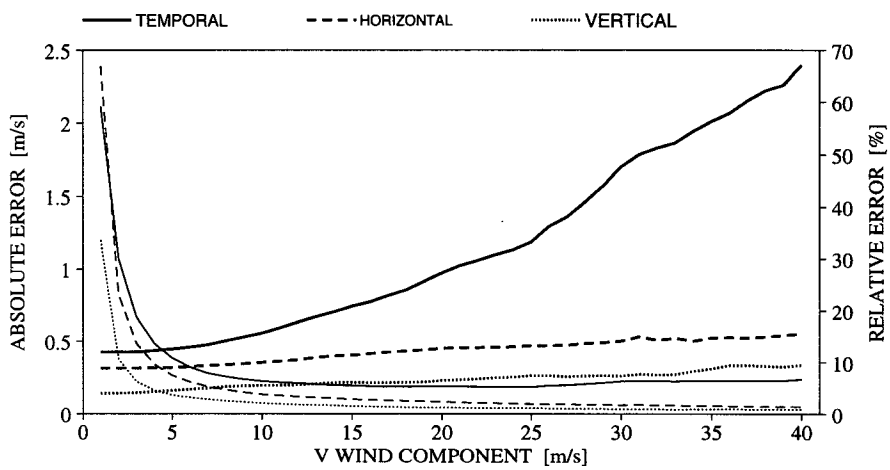

FIG. 2. Dependence of the different contributions to the total interpolation error on wind speed for the v wind component for 6-h temporal and 2.0° horizontal resolution and with nine vertical levels. Interpolation methods are bicubic for horizontal, quadratic for vertical, and linear for temporal interpolation. Absolute errors are given as bold lines, relative errors as thin lines.

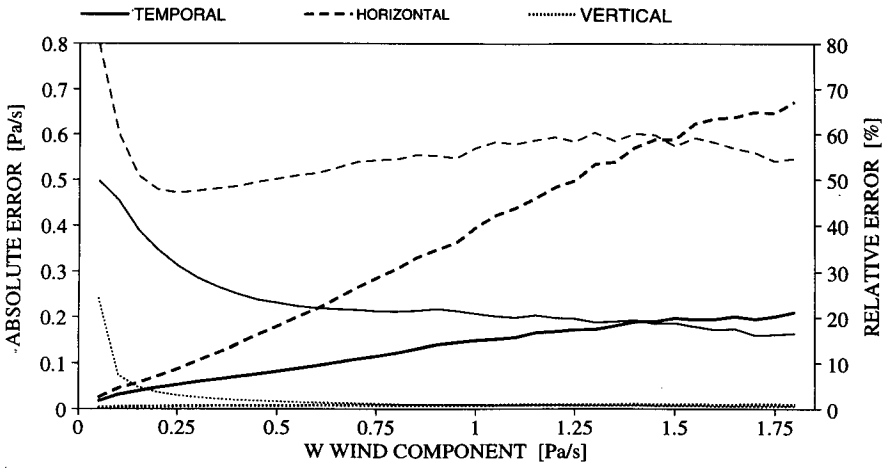

FIG. 3. Same as Fig. 2 but for the w component.

$$\epsilon_r(x, y, z, t) = \frac{2|s_r(x, y, z, t) - s_i(x, y, z, t)|}{|s_r(x, y, z, t)| + |s_i(x, y, z, t)|}, \tag{5}$$

where ϵ_r varies between 0 (for $s_r = s_i$) and 2 [for $\mathrm{sgn}(s_r) \neq \mathrm{sgn}(s_i)$]. Both interpolation errors were averaged over the whole fine grid (including the points of the coarse grid), and standard deviations and maximum values were calculated. Only the mean errors shall be discussed here because those interpolation techniques that gave the smallest mean errors also yielded the smallest standard deviations and in general the smallest maximum errors.

Four days were arbitrarily selected (1 May, 1 August, 1 November 1992, and 1 February 1993), and for each day nine wind fields in 3-h intervals centered above central Europe, with 241 × 121 × 17 grid points (height of the top level approximately 8000 m), were extracted from the ECMWF database. Figure 1 presents charts of the 1200 UTC geopotential at 500 hPa for the 4 days. The synoptic situations were very different from each other. Nevertheless, results of the interpolation experiments discussed below were similar for the individual days, with differences for ϵ_r being smaller than those for ϵ_a. Therefore, results from the interpolation experiments with this 4-day sample should be sufficiently representative.

From these fields, eight subgrids with 240 × 120 × 16 grid points were reconstructed by interpolation from the degraded fields. The degradation of the wind fields is described in more detail in the following sections. The points along one border in space and time were excluded because otherwise too much weight would have been given to grid points with zero interpolation error. The mean zonal and meridional wind component $\overline{|v_i|}$ were 8.4 and 6.4 m s^{-1}, respectively. The mean vertical wind component was 0.13 Pa s^{-1}.

The interpolation process was split into three steps that were treated separately: horizontal interpolation (HI), vertical interpolation (VI), and temporal interpolation (TI).

a. Horizontal interpolation

For HI, the following frequently used techniques were examined:

1) Nearest neighbor (NN): s_i is the value of the closest grid point.

2) Linear weighted distance (LWD): the surrounding four grid points are weighted linearly with their inverse distance. This method is not recommended for interpolation in a regular grid as it produces discontinuous results, but is frequently used for interpolation of irregularly spaced measurements.

3) Bilinear interpolation (BI) [Press et al. 1992, Eq. (3.6.5)].

4) Quadratic interpolation (QU) (Press et al. 1992, 102–104): sequential application of one-dimensional quadratic polynomials.

5) Bicubic interpolation (BC) (Press et al. 1992, 118–120), which also uses the cross derivatives of the function.

The horizontal resolution was reduced from 0.5° to 3.0° in steps of 0.5°. Table 1 shows the errors resulting from the different interpolation methods. The simple nearest neighbor and the linear weighted distance interpolation lead to interpolation errors of more than 10% for the horizontal wind components and more than 30% for the vertical wind component (for the 1.0° grid). The bilinear interpolation performs much better and even more so the higher-order interpolation methods. This is in good agreement with the findings of Walmsley and Mailhot (1983). The smallest errors occur with the bicubic interpolation. With this method, ϵ_a for 1.0° resolution is only 0.06 m s^{-1}, that is, less than 1% of the mean $u(v)$ wind components, ϵ_r is approximately 3% for both wind components. By further

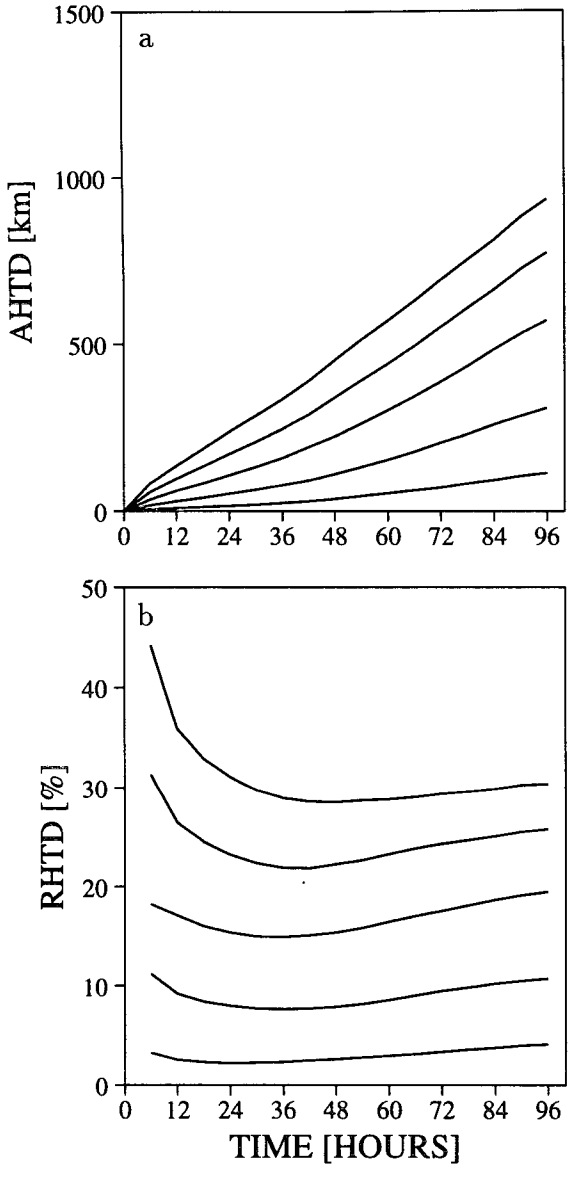

FIG. 4. (a) Absolute (AHTD) and (b) relative (RHTD) transport deviations for 2D trajectories calculated on grids of 1.0°, 1.5°, 2.0°, 2.5°, and 3.0° resolution, respectively. The lowest curves are for the 1.0° grid, the uppermost for the 3.0° grid.

reducing the grid resolution to 3.0°, ϵ_a and ϵ_r grow fast to 0.70 m s^{-1} (0.90 m s^{-1}) and 26%, respectively.

Considering the w component, both ϵ_a and ϵ_r are much larger, starting at ϵ_a = 0.02 Pa s^{-1} (i.e., 12% of mean w) and ϵ_r = 22% for 1.0° resolution, and reaching as much as ϵ_a = 0.10 Pa s^{-1} (i.e., 77% of mean w) and ϵ_r = 86% for 3.0° resolution (bicubic interpolation). The large interpolation errors in w are due to the high-frequency spatial variability of w.

Table 2 compares the computational efficiency of the five interpolation techniques. It is obvious that greater accuracy has its price. The bicubic interpolation takes 36 times longer than the simple nearest neighbor interpolation and 12 times longer than the bilinear interpolation. As the interpolation routines are one of the major CPU time-consuming parts of a trajectory model, this is directly related to the total CPU time consumption of the model.

b. *Vertical interpolation*

For the VI, methods NN, QU, and a linear interpolation (LI) were tested. The number of levels was reduced in three steps from 17 to 9, 5, and 3, respectively (Table 3). The VI errors for u and v are somewhat greater than the HI errors when reducing the resolution by a factor of 2 (i.e., comparison 9 levels versus 1.0°). This is especially valid for the higher-order interpolation techniques. Quadratic interpolation performs best with ϵ_a = 0.18 m s^{-1} [i.e., 2% (3%) of mean u (v)] and ϵ_r = 6% (7%).

In contrast to the results for u and v, the VI errors of w are smaller than those of the HI. Again, comparing a reduction in resolution by a factor of 2, ϵ_a of the VI (0.005 hPa s^{-1}) is smaller by a factor of 3 than ϵ_a of the HI. This is partly due to the fact that large variations in w are caused by orographic effects that lead to large HI but smaller VI errors. Nevertheless, the relative interpolation errors of w (ϵ_r = 13%) are much larger than those of u and v.

c. *Temporal interpolation*

For the TI the same methods as for the VI were examined. The time resolution was reduced from 3 to 6 and 12 h. Results are shown in Table 4. The nearest neighbor interpolation produced the worst results and, interestingly, for interpolation from the 6-h resolution, the linear method performs best, although the quadratic method is only marginally worse. With 6-h resolution and linear interpolation, ϵ_a is more than 0.5 m s^{-1} [i.e., 6% (8%) of the mean wind speed] and ϵ_r = 14% (17%) for u (v). For w, ϵ_a = 0.04 Pa s^{-1} (i.e., 29% of mean w) and ϵ_r = 42%. In addition, the standard deviation of ϵ_a is very high (0.08 Pa s^{-1}), indicating the frequent occurrence of substantial interpolation errors in the vertical wind.

d. *Dependence of the interpolation errors on wind speed*

The dependence of the interpolation errors on the wind speed was investigated for a combination of horizontal, vertical, and temporal resolutions for which, on average, each interpolation contributes equally to the total error. A temporal resolution of 6 h (linear interpolation), a horizontal resolution of 2° (bicubic interpolation), and 9 vertical levels (quadratic interpolation) were chosen. The errors ϵ_a and ϵ_r of the v wind component were plotted against wind speed (Fig. 2, results for u are similar). The largest contribution

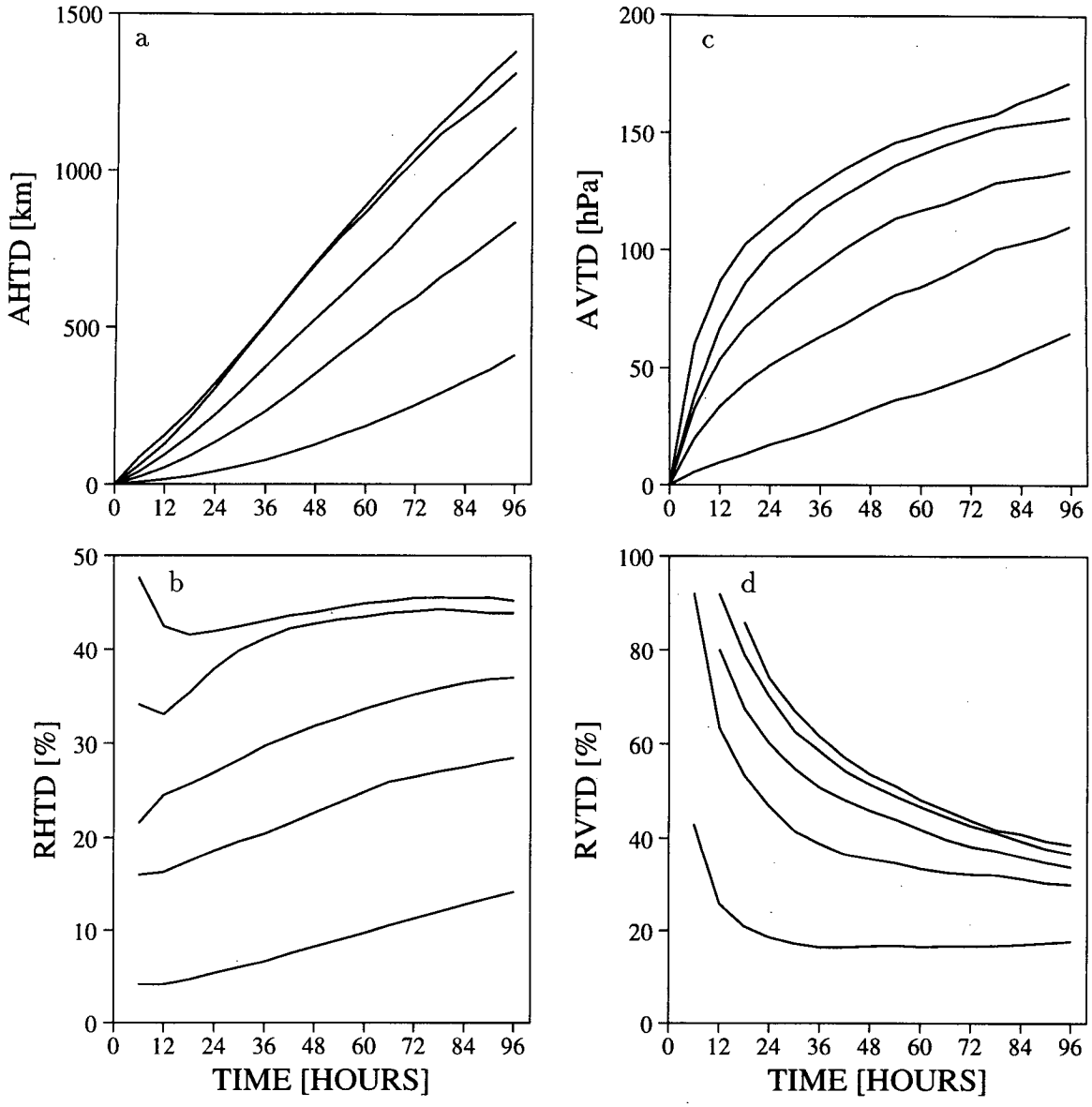

FIG. 5. (a) AHTD, (b) RHTD, (c) AVTD, and (d) RVTD for 3D trajectories resulting from HI. See also Fig. 4.

TABLE 5. Mean absolute (AHTD, AVTD) and relative (RHTD, RVTD) transport deviations after 96-h travel time for 2D and 3D trajectories, respectively. The first row indicates HI, VI, and TI, the second row gives the resolutions used in each case (for VI, the number of levels is given).

	HI	VI	TI	HI	VI	TI	HI	VI	TI
	1°	11	6 h	2°	6	12 h	3°	4	24 h
AHTD, 2D (km)	111	172	277	570	656	612	933	724	882
RHTD, 2D (%)	4.1	5.8	8.8	19.5	24.4	20.1	30.4	27.8	29.5
AHTD, 3D (km)	411	316	595	1139	716	894	1378	907	1145
AVTD, 3D (hPa)	64	49	84	133	89	107	171	101	122
RHTD, 3D (%)	14.1	11.5	19.8	37.1	26.0	30.3	45.3	34.0	38.2
RVTD, 3D (%)	17.5	13.6	23.7	33.6	25.9	30.7	38.6	29.6	35.8

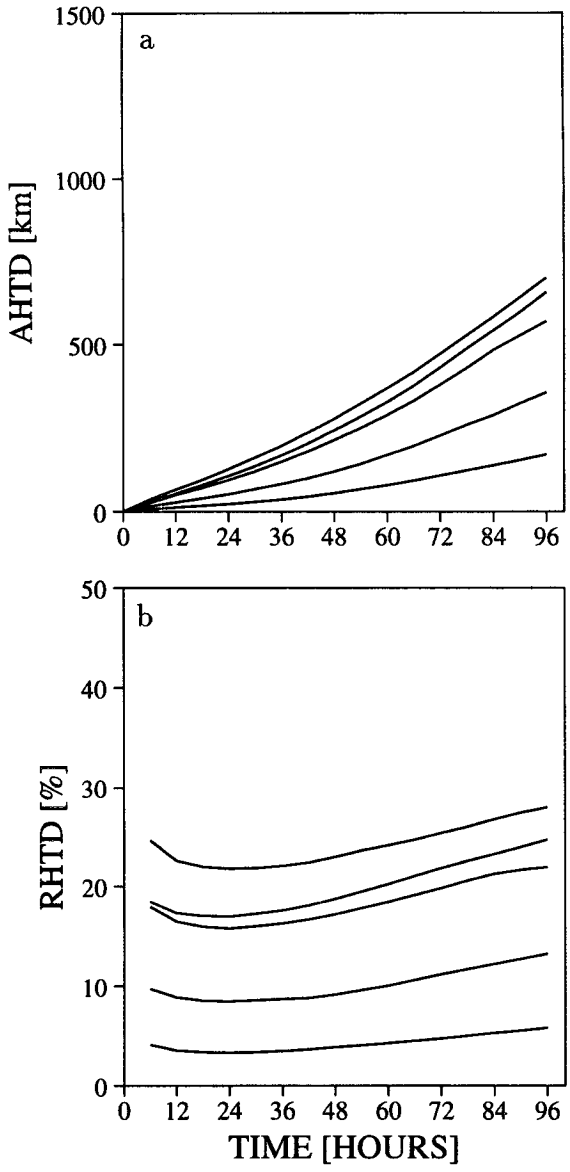

FIG. 6. (a) AHTD and (b) RHTD for 2D trajectories resulting from VI, calculated from grids with the number of levels reduced by a factor of 2, 3, 4, 5, and 6, respectively.

to the total error is by the TI, followed by HI and VI. This is valid for all wind speeds, but while ϵ_a for the spatial interpolations has a slow and linear increase, ϵ_a for the TI has a strong and nonlinear increase with wind speed. Therefore, differences between spatial and temporal interpolation are greatest for the highest wind speeds. This is understandable as local changes are fast with high wind speeds, while the spatial structures of the wind fields usually are large enough to be sufficiently resolved.

Relative interpolation errors grow very large for low wind speeds. While the spatial ϵ_r decreases monotonously with wind speed, the temporal ϵ_r has a minimum at 25 m s^{-1} and increases slightly for higher wind speeds. For high wind speeds, the temporal interpolation dominates the total interpolation error and the spatial interpolation errors are much less important. These results indicate that for a trajectory model with, for example, 2° resolution, a temporal resolution of 6 h is adequate (in terms of equal contribution to the total interpolation error) only for low wind speeds, while for higher wind speeds the temporal resolution is too low.

An analogous investigation was done for the vertical wind component. Here the HI is the limiting factor. While the VI error is negligible, ϵ_a for the HI increases sharply with vertical wind speed (Fig. 3). Even ϵ_r is increasing for wind speeds above 0.2 Pa/s, being generally well above 50%.

4. Effects of wind field interpolation errors on trajectory accuracy

In section 3 we found that considerable errors in the interpolation of the wind field occur. In this section the effect of these errors on the accuracy of trajectories shall be examined. For this purpose, Kahl and Samson (1986) integrated normally distributed random errors along trajectories, taking the magnitude of these errors from their interpolation experiments. This approach, however, is not very satisfying. An interpolation error leads to a position error of the trajectory, which in turn leads to the use of erroneous wind data for the next integration step (even with a hypothetically zero interpolation error). Because this process has been neglected by Kahl and Samson (1986), their method underestimates the trajectory errors.

In this work, the method of Rolph and Draxler (1990) was adopted. High-resolution wind fields (0.5°, 21 levels, 3-h time resolution) were used to construct reference trajectories against which trajectories computed from degraded wind fields were compared. In accordance with Kuo et al. (1985) and Rolph and Draxler (1990), absolute horizontal (AHTD, given in kilometers) and vertical (AVTD, given in hectopascals) transport deviations were defined as

$$\mathrm{AHTD}(t) = \frac{1}{N}\sum_{n=1}^{N} \{[X_n(t) - x_n(t)]^2 + [Y_n(t) - y_n(t)]^2\}^{1/2}$$

$$\mathrm{AVTD}(t) = \frac{1}{N}\sum_{n=1}^{N} |P_n(t) - p_n(t)|, \qquad (6)$$

where N is the total number of trajectories, X, Y, and P are the locations of the reference trajectories, and x, y, and p are the locations of the "degraded" trajectories at travel time t. In addition, a relative horizontal transport deviation

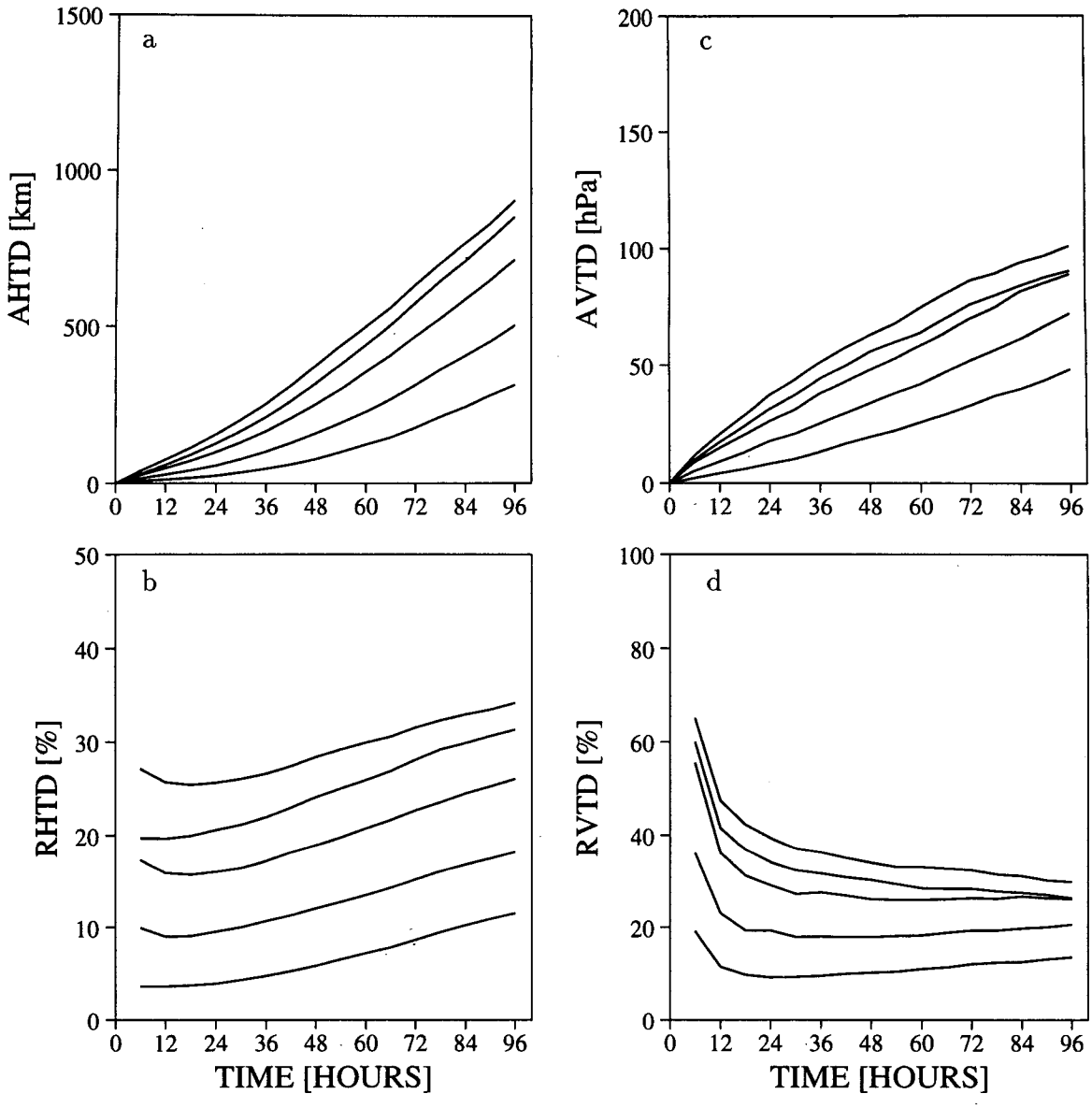

FIG. 7. (a) AHTD, (b) RHTD, (c) AVTD, and (d) RVTD for 3D trajectories resulting from VI. See also Fig. 6.

$$\mathrm{RHTD}(t) = \frac{1}{N}\sum_{n=1}^{N} \frac{\{[X_n(t) - x_n(t)]^2 + [Y_n(t) - y_n(t)]\}^{1/2}}{\mathrm{LH}_n(t)}$$

was introduced, with

$$\mathrm{LH}_n(t) = \frac{1}{2}\sum_{t_i=1}^{t} \langle \{[X_n(t_i) - X_n(t_{i-1})]^2 + [Y_n(t_i) - Y_n(t_{i-1})]^2\}^{1/2} + \{[x_n(t_i) - x_n(t_{i-1})]^2 + [y_n(t_i) - y_n(t_{i-1})]^2\}^{1/2}\rangle. \quad (7)$$

The relative vertical transport deviation was defined as

$$\mathrm{RVTD}(t) = \frac{1}{N}\sum_{n=1}^{N} \frac{|P_n(t) - p_n(t)|}{\mathrm{LV}_n(t)},$$

with

$$\mathrm{LV}_n(t) = \frac{1}{2}\sum_{t_i=1}^{t} [|P_n(t_i) - P_n(t_{i-1})| + |p_n(t_i) - p_n(t_{i-1})|]. \quad (8)$$

These relative transport deviations are analogous to the relative error defined for the interpolation experi-

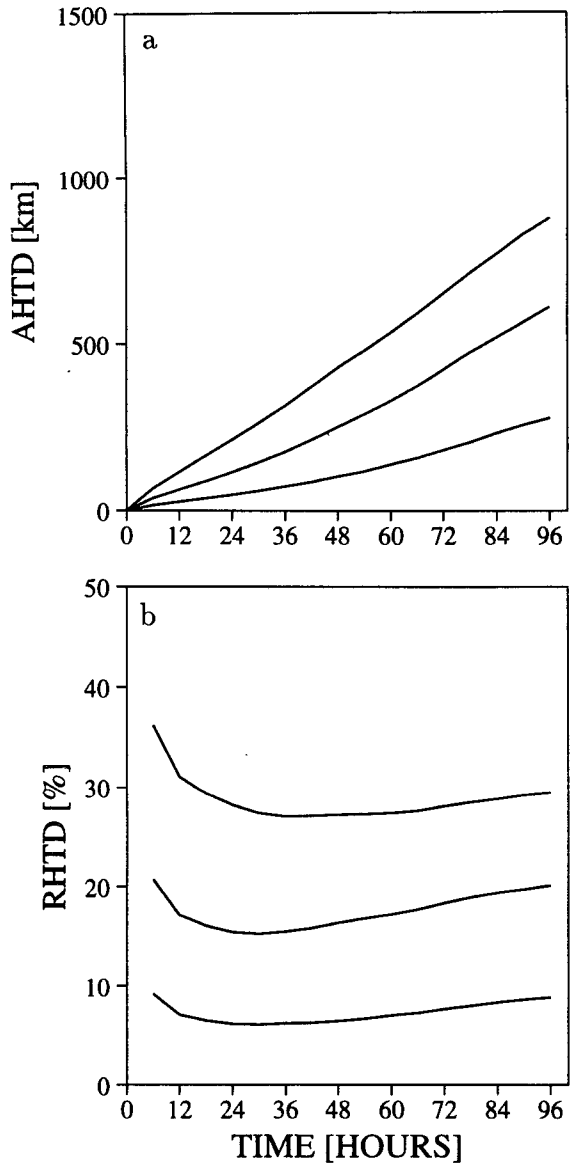

FIG. 8. (a) AHTD and (b) RHTD for 2D trajectories resulting from TI, calculated from grids with 6-, 12-, and 24-h resolution, respectively.

ments of section 3, yielding a maximum deviation of 2 for trajectories heading into opposite directions. Rolph and Draxler (1990) used a somewhat different formulation of the relative transport deviation. Tests showed that on the average their formula yields approximately 20%–30% smaller deviations than the one used here. However, bearing this in mind, results can be compared.

For the period July to December 1993, four daily trajectories were calculated with the starting position of Vienna (48°N, 16°E) and a length of 96 h forward in time. Trajectories were started at altitudes of 1000, 2000, and 5000 m above sea level, corresponding to 400, 1400, and 4400 m above model ground, respectively. This yielded a total number N of 2211 trajectories of each kind. The positions of the reference and the "degraded" trajectories were compared every 6 h. Two different types of trajectories were examined: 3D and isoeta (2D) trajectories. Again, errors due to HI, VI, and TI were investigated separately. Vienna is situated eastward of the Alps. As the majority of the trajectories travel eastward, most of the trajectories do not cross the Alps. A certain fraction, however, does. Interpolation of the w component will be especially difficult in these cases, leading to larger than average transport deviations.

a. Horizontal interpolation

In the horizontal, the bicubic interpolation was used, which has the smallest errors according to section 3. The grid resolution was reduced in five experiments from 0.5° to 3.0° in steps of 0.5°. Figures 4 and 5 show the resulting transport deviations for 2D and 3D trajectories, respectively. As expected, transport deviations increase strongly with decreasing grid resolution (Table 5).

For 2D trajectories, AHTD increase linearly with transport time, while RHTD are more or less constant. RHTD for 1.0° grid resolution are comparatively small (<5%), but a further reduction of the resolution yields more severe transport deviations, namely almost 20% for 2.0° and 30% for 3.0°, respectively (Table 5).

For 3D trajectories, deviations due to decreased resolution are much larger than for 2D trajectories. Even with the 1.0° grid resolution AHTD exceeds 400 km after 96-h travel time. RHTD increases with travel time in the 3D case, especially for high grid resolutions. Vertical transport deviations are even worse than the horizontal ones. An AVTD of nearly 60 hPa is observed after 96-h travel time, even with 1.0° grid resolution. RVTD is around 20% for 1.0° grid resolution and more than 30% for 2.0° resolution after 96-h travel time.

These results are consistent with the findings of section 3, as it was shown there that relative interpolation errors in w are much greater than those in u and v. The large interpolation errors in w first lead to an erroneous height of the trajectory. Further on, also the horizontal position is affected with u and v being taken from an incorrect height. This mechanism leads to an increasing RHTD with travel time, in contrast to the findings for the 2D trajectories (Figs. 4 and 5).

Absolute transport deviations are larger for the 5000-m starting level than for the 1000-m level, while the relative deviations at the upper level are somewhat smaller. This is due to the higher wind speeds at higher levels. However, differences are not too great and are therefore not shown separately.

The transport errors found in this paper are much larger than those published by Rolph and Draxler (1990), who computed 3D trajectories in the boundary layer for a travel time of 96 h. They found AHTD and

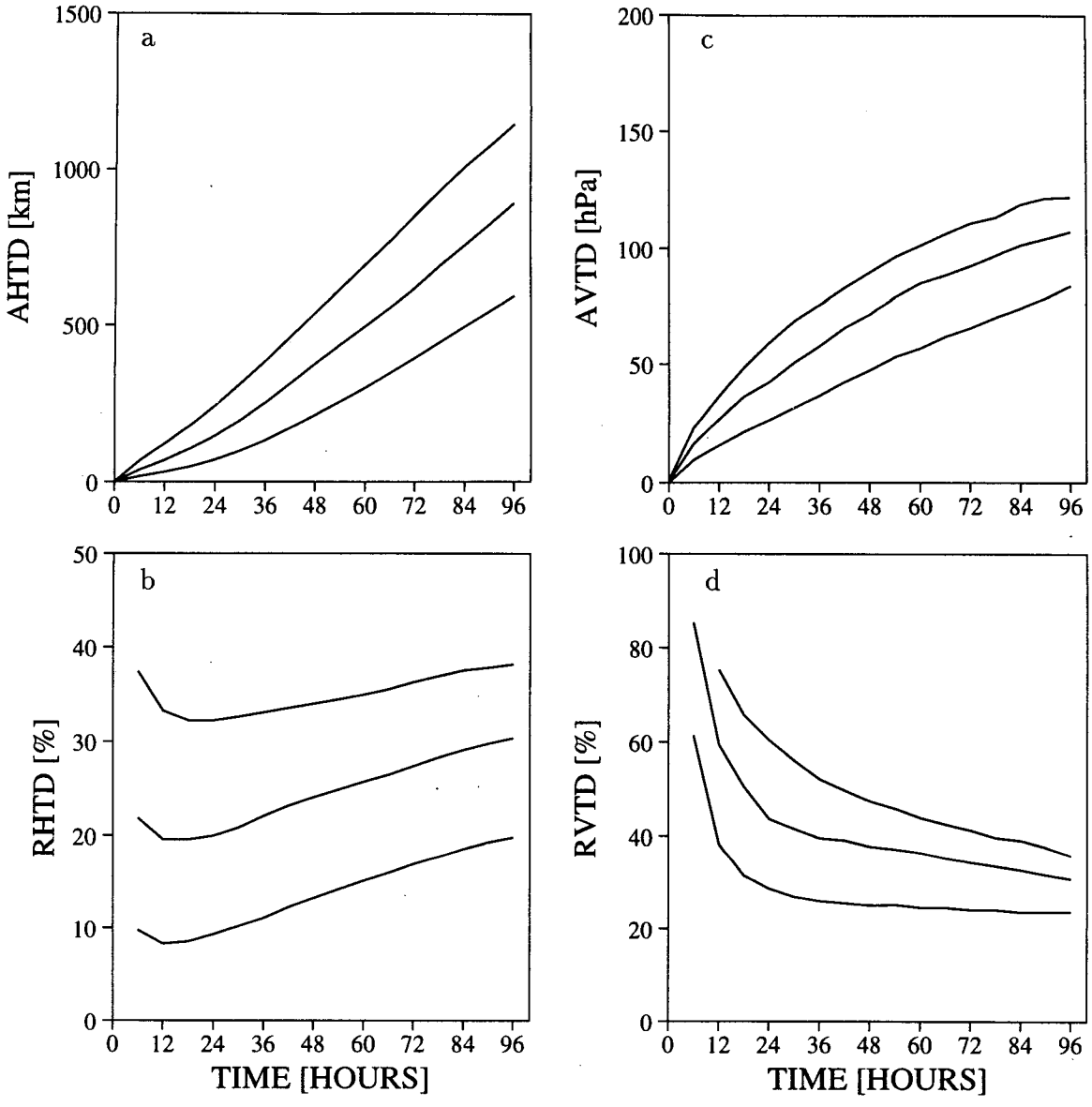

FIG. 9. (a) AHTD, (b) RHTD, (c) AVTD, and (d) RVTD for 3D trajectories resulting from TI. See also Fig. 8.

AVTD of slightly more than 400 km and 30 hPa for a reduction of the horizontal grid resolution from 90 to 360 km using bilinear interpolation. The corresponding relative deviations were both around 15%. On the other hand, for a resolution reduction from 0.5° to 2.0°, in this work an AHTD of 1140 km and an RHTD of 37% was found. There are several explanations for this discrepancy. First, the AHTD found by Rolph and Draxler were lower because they used only boundary layer trajectories, whereas here trajectories at higher starting levels were also used, which have higher AHTD due to higher wind speeds. Second, Rolph and Draxler treated their fields with a 180-km smoothing operator, thus reducing the small-scale variability. This will affect especially the vertical wind, which has the highest variability. Third, as the definition of the RHTD in this work leads to values higher by 20%–30% than Rolph and Draxlers formulation, this adds to the differences in the RHTD.

Fourth, an additional reason is the specific starting location eastward of the Alps used in this work. Over the Alps, interpolation is especially critical because of the more complex airflow. Therefore, trajectories crossing the Alps should have higher transport deviations. To test this hypothesis, the dataset was split into trajectories traveling over the Alps and others. For the trajectories crossing the Alps, the AHTD after 96-h travel time and for a grid resolution of 2° was 1331

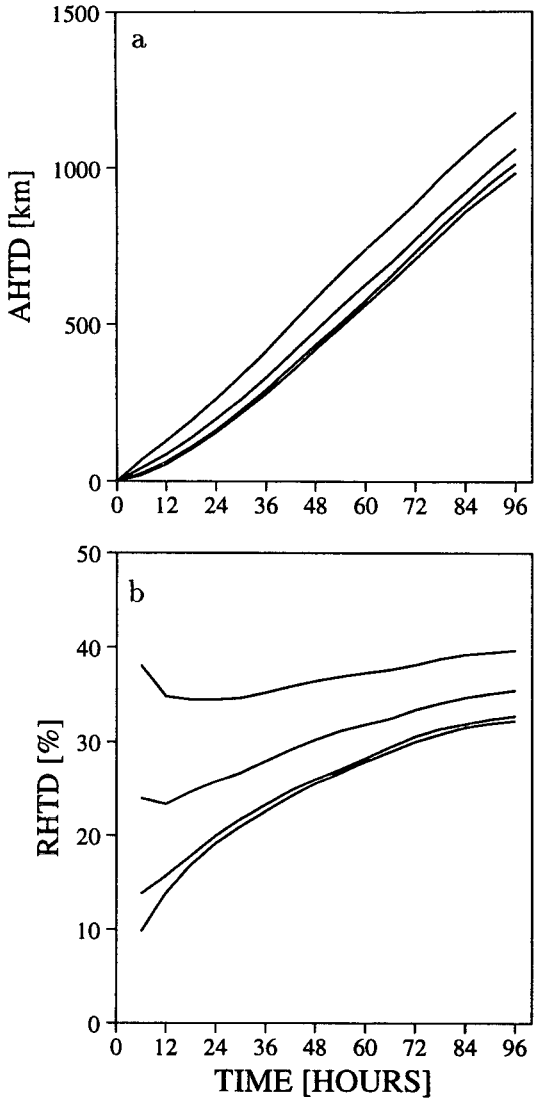

FIG. 10. (a) AHTD and (b) RHTD between 2D trajectories computed from wind fields with a resolution of 3, 6, 12, and 24 h, respectively, with respect to 3D trajectories computed from wind fields with 3-h resolution.

km, whereas for the others it was only 963 km. As the fraction of trajectories traveling over flatlands was higher in the work of Rolph and Draxler, this also explains some part of the differences between their results and those found here.

b. *Vertical interpolation*

In the vertical, quadratic interpolation (QU) was applied. Twenty-one levels were used for the computation of the reference trajectories. In five experiments, wind data were taken only from every second, third, fourth, fifth, and sixth level, respectively, plus the uppermost level. A decrease of the number of levels by a factor of 2 yielded an AHTD of 172 km and a RHTD of 5.8% after 96-h travel time of the 2D trajectories (Table 5). This is slightly more than the transport deviations resulting from a horizontal resolution reduction from 0.5° to 1.0°. However, further reduction of the number of levels does not affect trajectory accuracy as much as a further reduction of horizontal resolution (Fig. 6).

For the 3D trajectories, the horizontal transport deviations are not much greater than for the 2D trajectories (Fig. 7) and are significantly smaller than the deviations produced by the HI. This is consistent with the finding of section 3 that VI of w produces relatively small errors.

c. *Temporal interpolation*

For TI linear interpolation was selected. The temporal resolution was reduced from 3 to 6, 12, and 24 h, respectively. As 6-h intervals of input wind fields are frequently used for trajectory calculations, only this case shall be discussed here.

For 2D trajectories (Fig. 8), after 96-h travel time, an AHTD of 277 km and a RHTD of 8.8% was found. For 3D trajectories (Fig. 9), the respective values are 595 km and 19.8%. After 24 h the AHTD increases linearly with almost 150 km day^{-1}. This is close to the overall error found by Haagenson et al. (1990) for boundary layer trajectories in comparison to tracer-derived trajectories. Although the AHTD after 96 h for the lowest starting point alone is somewhat less (493 km), these results show that TI of w has to be considered a significant source of error for trajectory computations. As spatial interpolation adds even more uncertainty, one may conclude that 3D trajectories have to be treated with care. Although in theory they should best represent the path of an air parcel, results can be severely impaired by interpolation errors if one has to rely on low-resolution wind fields, specifically with less than 0.5° and 3-h resolution.

The large temporal interpolation errors of the vertical wind component give rise to the question if 3D trajectories computed from wind fields with a certain temporal resolution are more accurate than the corresponding 2D trajectories. To answer this question, 3D trajectories computed from the grid with 0.5° spatial and 3-h temporal resolution were used as reference trajectories also for 2D trajectories computed from the 0.5° resolution grids and 3-, 6-, 12-, and 24-h temporal resolution (Fig. 10). The AHTDs after 96-h travel time were approximately 1000 km, being nearly independent of the temporal resolution. The AHTDs of the 3D trajectories were of similar magnitude for 24- and 12-h resolution, but less for 6-h resolution. If the high-resolution 3D trajectories are considered as the ones that come closest to the "true" trajectories, the conclusion can be drawn that although 3D trajectories with 6-h resolution are subject to large interpolation errors,

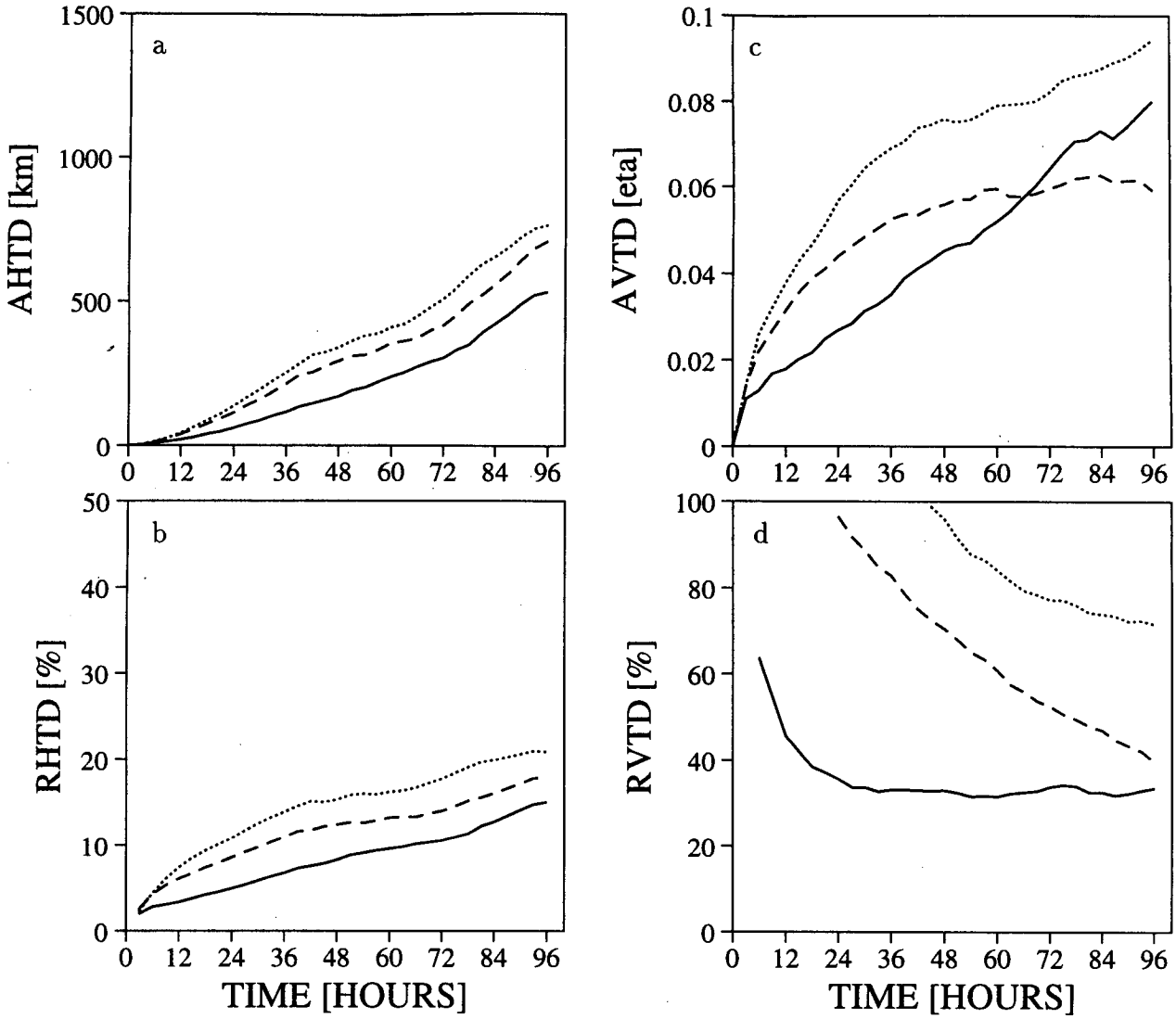

FIG. 11. (a) AHTD, (b) RHTD, (c) AVTD, and (d) RVTD between 3D and isentropic (solid lines), isentropic, and isoeta (dashed), and 3D and isoeta (dotted) trajectories. AVTD is given in eta units.

they are still more accurate than corresponding 2D trajectories.

5. Comparison of different types of trajectories

As FLEXTRA allows the calculation of several types of trajectories within one model run and with the same input data, a comparison of 3D, isentropic, isoeta, and BL trajectories will be presented. It is difficult to determine the absolute accuracy of trajectories and no attempt is made here to assess it. However, an intercomparison of trajectories allows an estimate of the uncertainties involved in the selection of a certain type of trajectory.

Trajectories were computed for the same period as in section 4 and for the same starting location. Three-dimensional, isentropic, and isoeta trajectories were compared for a starting level of 5000 m. Conservation of potential temperature, as assumed for isentropic trajectories, is fulfilled only for adiabatic and inviscid motions. Therefore, regions of the atmosphere where diabatic processes cannot be neglected were excluded from the investigation. Trajectories were terminated when they approached the ground to more than 3200 m to avoid diabatic processes in the boundary layer. Trajectories were also terminated if they entered regions with relative humidity exceeding 95% as latent heat may be released or consumed there.

The comparison showed that transport deviations, both horizontal and vertical, between 3D and isentropic trajectories are smaller than deviations between isoeta trajectories and the other types (Fig. 11). This confirms

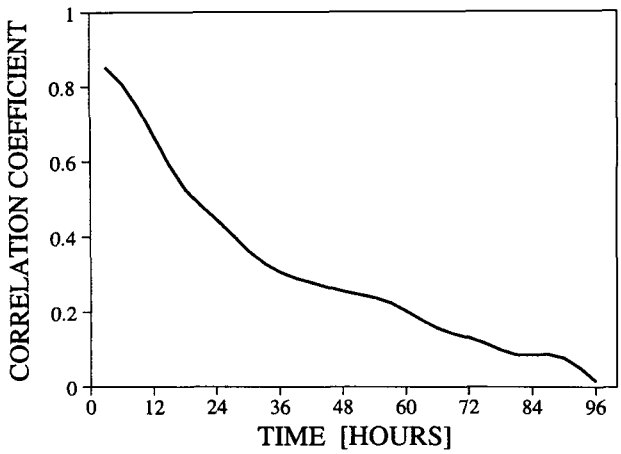

FIG. 12. Correlation coefficient between the vertical motions of 3D and isentropic trajectories.

that vertical transports as simulated by 3D and isentropic trajectories are comparable for adiabatic motions. In Fig. 12 the correlation coefficients between the vertical motion $[z(t) - z(t - 3\text{ h})$, with z being height] of 3D and isentropic trajectories within 3-h intervals are shown. During the first 3 h of transport, the vertical displacements are highly correlated ($r = 0.85 \pm 0.07$). However, r declines fast to less than 0.3 after 48 h. This is easily understandable as horizontal and vertical transport errors occur along the trajectory and add to the differences. In general, 3D trajectories tend to have more pronounced vertical motions than isentropic trajectories.

An additional comparison was made for trajectories within the boundary layer where 3D, isoeta, and BL trajectories were compared. Three-dimensional and isoeta trajectories were started at a height of 400 m above the topography, and for BL trajectories, mixing height was set constant to 1000 m. One can see from Fig. 13 that isoeta and BL trajectories agree reasonably well. After 96-h travel time their AHTD has grown to approximately 400 km, while their RHTD stays nearly constant (15%) with travel time. Keeping in mind the large errors that occur from other sources such as interpolation and wind field errors, these deviations seem acceptable. More severe are the deviations between 3D and the other trajectories. In both comparisons an AHTD of nearly 900 km results after 96-h travel time, and the RHTD exceeds 30% after 65-h travel time. These deviations are even more severe than those found for trajectories in the free troposphere and can be explained by the strong vertical wind shear within the BL under stable conditions.

6. Discussion and conclusions

The main results can be summarized as follows:

1) Interpolation errors in wind fields can be substantial. For gridded output fields of the ECMWF model interpolation errors due to temporal interpolation are larger than those due to spatial interpolation.

2) Interpolation of the vertical wind component leads to errors much greater than those of the interpolation of the horizontal components. For example, a reduction of the temporal resolution from 3 to 6 h leads to a mean relative interpolation error of 40% for w. This is due to the high-frequency variability of the w fields.

3) For spatial interpolation, higher-order interpolation schemes (bicubic in the horizontal, second-order polynomial in the vertical) reduce interpolation errors as compared to linear interpolation. Contrarily, for temporal interpolation, higher-order interpolation

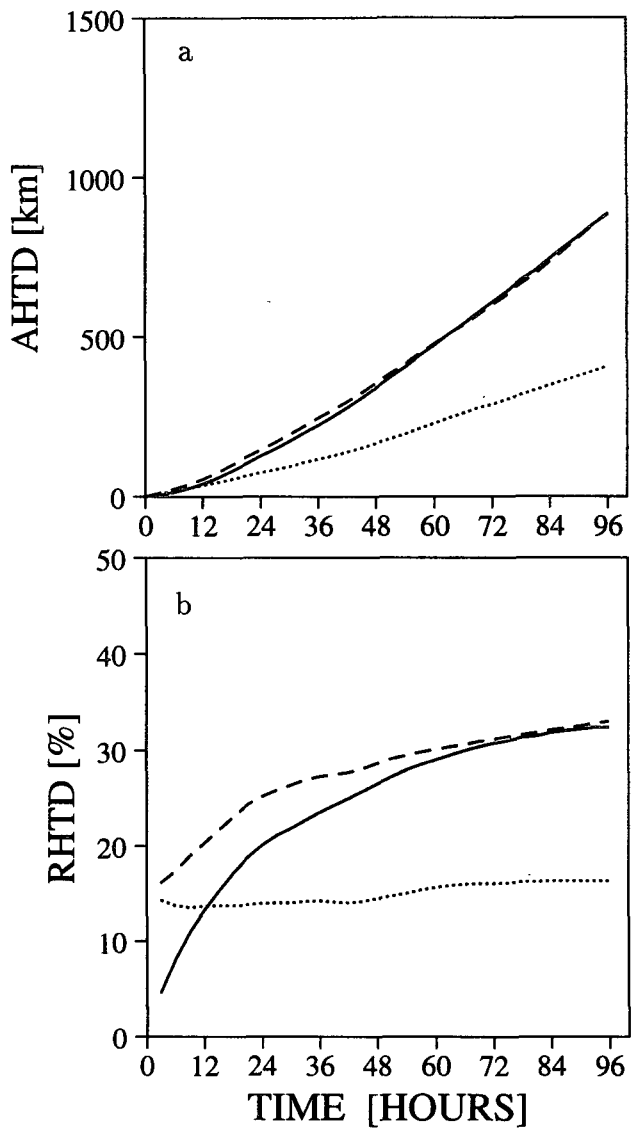

FIG. 13. (a) AHTD and (b) RHTD between 3D and isoeta (solid lines), 3D and boundary layer (dashed), and isoeta and boundary layer (dotted) trajectories.

schemes do not reduce interpolation errors. This is probably due to the low temporal resolution of the wind fields. With higher resolution (probably around 1 h), results might resemble those for spatial interpolation.

4) Absolute interpolation errors increase, but relative errors decrease with wind speed.

5) Interpolation errors can severely impair the accuracy of trajectories, especially of 3D trajectories. While for isoeta trajectories, the AHTD after 96 h due to TI of 6-h wind fields was 280 km, the corresponding AHTD for 3D trajectories was 600 km (i.e., a RHTD of 20%).

6) Transport deviations due to reduced grid resolution are more severe for trajectories crossing the Alps than for others. For example, after 96-h travel time and 1° grid resolution, the AHTD was 509 km for trajectories that crossed the Alps, but only 324 km for those that did not.

7) Transport deviations between different types of trajectories are significant when compared with errors due to interpolation.

It may be of interest to note that the large temporal interpolation errors could be reduced if the wind data available were time averages over the interval between the times when such fields are available. Typical NWP model output, however, consists of instantaneous values that are needed for synoptical analyses. The advantage of time-averaged wind fields can be demonstrated for the special case of spatially homogeneous wind fields if we view the wind component $u(t)$ at a certain time t as the sum of a mean part $\bar{u}$ averaged between times t_0 and t_1 and a perturbation part $u'(t)$. If we consider the integration of the trajectory equation between t_0 and t_1, then

$$x(t_1) - x(t_0) = \int_{t_0}^{t_1} u(t)dt = \bar{u}(t_1 - t_0), \quad (9)$$

which means that for wind fields that are averaged between t_0 and t_1 the trajectory position error is zero. On the other hand, if an instantaneous wind field is given at time $(t_0 + t_1)/2$, a position error $(t_1 - t_0)u'[(t_0 + t_1)/2]$ results.

From the findings of this work, the following conclusions can be drawn:

1) For the most economical use of computer resources, a balanced spatial and temporal resolution should be aimed at, with spatial and temporal interpolation contributing about equally to the total error. For example, for a temporal resolution of 6 h, 2° horizontal resolution and nine levels seem to be most appropriate. If the accuracy of trajectories is to be enhanced, spatial and temporal resolutions should be increased by approximately the same factor. An increase of spatial or temporal resolution alone also results in greater accuracy of the trajectories, but is less efficient.

2) For the currently available spatial resolution of the ECMWF T213 L31 model, it would be advantageous to reduce the time interval between model outputs from 3 to 1 h. Currently, the temporal resolution is the major limitation to the accuracy of trajectories.

3) In general, kinematic 3D trajectories are recommendable. However, if wind fields with sufficient resolution are not available, a computation of 2D trajectories is also appropriate. For example, in the synoptic scale and with a horizontal resolution of 0.5°, the resolution in time should be at least 6 h to adequately represent vertical motions.

4) To assess the sensitivity of trajectories in specific situations, it is highly recommendable to compute an ensemble of trajectories. Merrill et al. (1985) started a number of trajectories with displacements of the starting positions to assess the trajectory accuracy in specific cases. Another possibility would be to add random errors to the wind components at each time step. The magnitude of these random errors can be estimated from the interpolation experiments of this study. This procedure would allow to assess the effect of interpolation errors on trajectory accuracy.

Acknowledgments. This work was made possible by funding from the Austrian Ministry of Science and Research as part of the Pannonian Ozone Project (POP) and the Austrian Fonds zur Förderung der wissenschaftlichen Forschung under Grant P7809 GEO. We thank L. Haimberger for giving us an extensive introduction to the ECMWF model and for providing the programs to extract $\dot{\eta}$, and N. Kreitz from the ECMWF for his assistance concerning data management. Without the help of these people this work would not have been possible.

REFERENCES

Artz, R., R. A. Pielke, and J. Galloway, 1985: Comparison of the ARL/ATAD constant level and the NCAR isentropic trajectory analyses for selected case studies. *Atmos. Environ.*, **19**, 47–63.

Danielsen, E. F., 1961: Trajectories: Isobaric, isentropic and actual. *J. Meteor.*, **18**, 479–486.

DeLeeuw, F. A., A. M. Van Rheineck, H. J. Leyssius, and P. J. H. Builtjes, 1990: Calculation of long term averaged ground level ozone concentrations. *Atmos. Environ.*, **24A**, 185–193.

Dorling, S. R., T. D. Davies, and C. E. Pierce, 1992: Cluster analysis: A technique for estimating the synoptic meteorological controls on air and precipitation chemistry—Method and applications. *Atmos. Environ.*, **26A**, 2575–2581.

Draxler, R. R., 1987: Sensitivity of a trajectory model to the spatial and temporal resolution of the meteorological data during CAPTEX. *J. Climate Appl. Meteor.*, **26**, 1577–1588.

ECMWF, 1989: *Research Manual 2. ECMWF Forecast Model—Adiabatic Part.* 2d ed. European Centre for Medium-Range Weather Forecasts.

Eliassen, A., and J. Saltbones, 1983: Modelling of long-range transport of sulphur over Europe: A two year model run and some model experiments. *Atmos. Environ.*, **17**, 1457–1473.

Haagenson, P. L., Y. H. Kuo, M. Skumanich, and N. L. Seaman, 1987: Tracer verification of trajectory models. *J. Climate Appl. Meteor.*, **26**, 410–426.

——, K. Gao, and Y.-H. Kuo, 1990: Evaluation of meteorological analyses, simulations, and long-range transport using ANATEX surface tracer data. *J. Appl. Meteor.*, **29**, 1268–1283.

Kahl, J. D., and P. J. Samson, 1986: Uncertainty in trajectory calculations due to low resolution meteorological data. *J. Climate Appl. Meteor.*, **25**, 1816–1831.

——, J. M. Harris, G. A. Herbert, and M. P. Olson, 1989: Intercomparison of long-range trajectory models applied to arctic haze. *Proceedings of the 17th NATO/CCMS ITM on Air Pollution Model, and Its Applications*, Plenum Press, 175–185.

Klug, W., 1992: *Evaluation of Long Range Atmospheric Transport Models Using Environmental Radioactivity Data from the Chernobyl Release.* Elsevier Science Publ., 366 pp.

Kuo, Y.-H., M. Skumanich, P. L. Haagenson, and J. S. Chang, 1985: The accuracy of trajectory models as revealed by the observing system simulation experiments. *Mon. Wea. Rev.*, **113**, 1852–1867.

Martin, D., C. Mithieux, and B. Strauss, 1987: On the use of the synoptic vertical wind component in a transport trajectory model. *Atmos. Environ.*, **21**, 45–52.

——, G. Bergametti, and B. Strauss, 1990: On the use of the synoptic vertical velocity in trajectory model: Validation by geochemical tracers. *Atmos. Environ.*, **24A**, 2059–2069.

McQueen, J. T., and R. R. Draxler, 1994: Evaluation of model back trajectories of the Kuwait oil fires smoke plume using digital satellite data. *Atmos. Environ.*, **28**, 2159–2174.

Merrill, J. T., R. Bleck, and L. Avila, 1985: Modeling atmospheric transport to the Marshall islands. *J. Geophys. Res.*, **90**, 12 927–12 936.

——, ——, and D. Boudra, 1986: Techniques of Lagrangian trajectory analysis in isentropic coordinates. *Mon. Wea. Rev.*, **114**, 571–581.

Petterssen, S., 1940: *Weather Analysis and Forecasting.* McGraw-Hill Book Company, Inc., 221–223.

Press, W. H., S. A. Teukolsky, W. T. Vetterling, and B. P. Flannery, 1992: *Numerical Recipes in FORTRAN. The Art of Scientific Computing.* 2d ed. Cambridge University Press, 963 pp.

Pudykiewicz, J., R. Benoit, and A. Staniforth, 1985: Preliminary results from a partial LRTAP model based on an existing meteorological forecast model. *Atmos.-Ocean*, **23**, 257–303.

Reisinger, L. M., and S. F. Mueller, 1983: Comparisons of tetroon and computed trajectories. *J. Climate Appl. Meteor.*, **22**, 664–672.

Rolph, G. D., and R. R. Draxler, 1990: Sensitivity of three-dimensional trajectories to the spatial and temporal densities of the wind field. *J. Appl. Meteor.*, **29**, 1043–1054.

Seibert, P., 1993: Convergence and accuracy of numerical methods for trajectory calculations. *J. Appl. Meteor.*, **32**, 558–566.

Stohl, A., and H. Kromp-Kolb, 1994: Origin of ozone in Vienna and surroundings, Austria. *Atmos. Environ.*, **28**, 1255–1266.

Walmsley, J. L., and J. Mailhot, 1983: On the numerical accuracy of trajectory models for long-range transport of atmospheric pollutants. *Atmos.-Ocean*, **21**, 14–39.